ACS Catalysis

Research Article

pubs.acs.org/acscatalysis

Mechanistic Study of Ru-NHC-Catalyzed Hydrodefluorination of Fluoropyridines: The Influence of the NHC on the Regioselectivity of C−F Activation and Chemoselectivity of C−F versus C−H Bond Cleavage

David McKay,[‡] Ian M. Riddlestone,[†] Stuart A. Macgregor,*[,‡] Mary F. Mahon,[†] and Michael K. Whittlesey*[,†]

[‡]Institute of Chemical Sciences, Heriot-Watt University, Edinburgh EH14 4AS, U.K.

[†]Department of Chemistry, University of Bath, Claverton Down, Bath BA2 7AY, U.K.

Supporting Information

ABSTRACT: We describe a combined experimental and computational study into the scope, regioselectivity, and mechanism of the catalytic hydrodefluorination (HDF) of fluoropyridines, $C_5F_{5-x}H_xN$ (x = 0−2), at two Ru(NHC)-$(PPh_3)_2(CO)H_2$ catalysts (NHC = IPr, **1**, and IMes, **2**). The regioselectivity and extent of HDF is significantly dependent on the nature of the NHC: with **1** HDF of C_5F_5N is favored at the *ortho*-position and gives 2,3,4,5-C_5F_4HN as the major product. This reacts on to 3,4,5-$C_5F_3H_2N$ and 2,3,5-$C_5F_3H_2N$, and the latter can also undergo further HDF to 3,5-$C_5F_2H_3N$ and 2,5-$C_5F_2H_3N$. *para*-HDF of C_5F_5N is also seen and gives 2,3,5,6-C_5F_4HN as a minor product, which is then inert to further reaction. In contrast, with **2**, *para*-HDF of C_5F_5N is preferred, and moreover, the 2,3,5,6-C_5F_4HN regioisomer undergoes C−H bond activation to form the catalytically inactive 16e Ru-fluoropyridyl complex Ru(IMes)$(PPh_3)(CO)$(4-C_5F_4N)H, **3**. Density functional theory calculations rationalize the different regioselectivity of HDF of C_5F_5N at **1** and **2** in terms of a change in the pathway that is operating with these two catalysts. With **1**, a stepwise mechanism is favored in which a N → Ru σ-interaction stabilizes the key C−F bond cleavage along the *ortho*-HDF pathway. With **2**, a concerted pathway favoring *para*-HDF is more accessible. The calculations show the barriers increase for the subsequent HDF of the lower fluorinated substrates, and they also correctly identify the most reactive C−F bonds. A mechanism for the formation of **3** is also defined, but the competition between C−H bond activation and HDF of 2,3,5,6-C_5F_4HN at **2** (which favors C−H activation experimentally) is not reproduced. In general, the calculations appear to overestimate the HDF reactivity of 2,3,5,6-C_5F_4HN at both catalysts **1** and **2**.

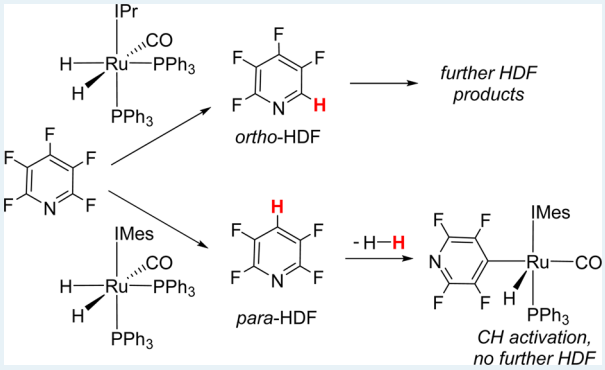

KEYWORDS: *catalysis, hydrodefluorination, DFT, mechanism, ruthenium, pentafluoropyridine, N-heterocyclic carbenes*

INTRODUCTION

Efforts to develop new synthetic routes to aromatic fluorocarbons are driven primarily by the important role that C−F-containing molecules occupy in the pharmaceutical and agrochemical industries, as exemplified by the molecules shown in Chart 1.[1] In the cases of compounds such as Tivicay or Sitagliptin,[2] one hypothetical approach to the preparation of the 2,4-difluorophenyl or 2,4,5-trifluorophenyl substituents would be via a metal-catalyzed hydrodefluorination (HDF) reaction of a pentafluorophenyl ring.[3]

However, significant obstacles first need to be overcome to realize such processes.[4] In most of the cases of either stoichiometric or catalytic C−F bond activation reported thus far, bond cleavage becomes more difficult as the number of fluorine substituents decreases, and so whereas transforming a -C_6F_5 group to a -C_6F_4H group is well-established, the second and third HDF steps that would be necessary to realize -$C_6F_3H_2$ and -$C_6F_2H_3$ groups are far more challenging.[5] Second, there needs to be control of regiochemistry to allow the targeted substitution of hydrogen atoms selectively into the desired positions. In the majority of catalytic HDF reactions that employ a simple model substrate such as C_6F_5H, functionalization of the C−F bond at the *para*-position takes place to generate 1,2,4,5-$C_6F_4H_2$.[3,6] This implies that even retaining the F *para* to the C−C bond in all three of the structures in Chart 1 might prove to be difficult, let alone the subsequent directed HDF at the *ortho*- and *meta*-positions. A third issue relates to chemoselectivity, in driving the more thermodynamically

Received: October 24, 2014
Revised: December 15, 2014
Published: December 16, 2014

DOI: 10.1021/cs501644r
ACS Catal. 2015, 5, 776−787

Chart 1. High-Value Fluoroaromatic Compounds

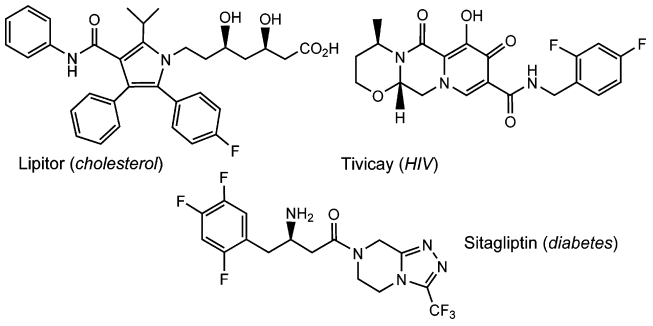

favorable C−F bond activation over the competitive and kinetically favored C−H activation.[7]

In 2009, we reported the catalytic HDF of C_6F_6, C_6F_5H and C_5F_5N by the ruthenium-based complexes Ru(NHC)-$(PPh_3)_2(CO)H_2$ (NHC = N-heterocyclic carbene) in the presence of alkylsilanes (Scheme 1). This system showed a very unusual and remarkably high regioselectivity for HDF at an *ortho*-position, for example, converting C_6F_5H to 1,2,3,4-$C_6F_4H_2$ with 98% selectivity.[8,9] Density functional theory (DFT) studies were able to explain this high *ortho*-selectivity on the basis of a novel nucleophilic hydride attack mechanism involving either a stepwise or concerted pathway.[10] In the former stepwise process (Pathway 1, Scheme 2), C_6F_5H initially binds in an η^2-fashion (**I**) which permits an intramolecular hydride attack to generate a metal-stabilized Meisenheimer intermediate (**II**). Loss of HF then produces an $L_nRu-C_6F_4H$ complex (**III**) which upon protonolysis eliminates 1,2,3,4-$C_6F_4H_2$. In the alternative concerted process (Pathway 2), direct Ru−H/C−F exchange takes place in an intermolecular fashion to generate 1,2,3,4-$C_6F_4H_2$ directly in a single step. For C_6F_5H, the stepwise pathway is more accessible. Moreover, the formation of the *ortho*-HDF product is favored over the *meta*- and *para*-isomers. This and subsequent work[11] also highlighted how Pathway 1 favors HDF at sites adjacent to a C−H bond, as this allows access to what would otherwise be a sterically encumbered transition state.

In the initial experimental study, we also showed that C_5F_5N was far more reactive than C_6F_5H in terms of activity (total TON) and in undergoing more than a single HDF step, resulting in the formation of trifluoro- and difluoropyridines. Using a combined experimental and computational approach, we now describe a study aimed at defining the scope, regioselectivity, and mechanism of HDF across a series of fluoropyridines using two Ru NHC catalysts, Ru(NHC)-$(PPh_3)_2(CO)H_2$ (NHC = IPr, **1** or IMes **2**[12]). The study

Scheme 2. Mechanisms of Ru-Catalyzed HDF of C_6F_5H to 1,2,3,4-$C_6F_4H_2$

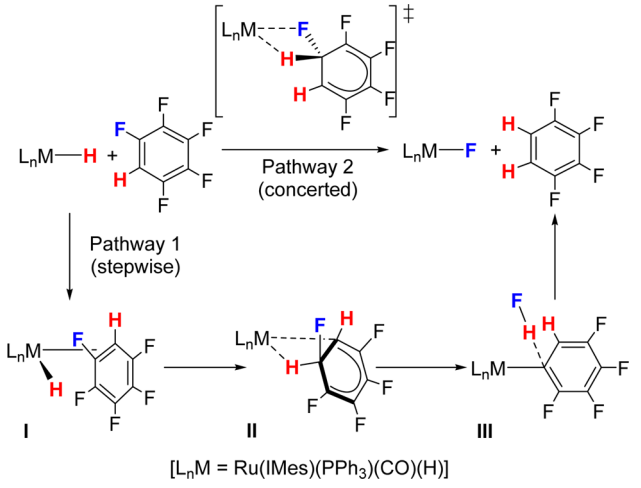

reveals that the change of NHC in these catalysts has a significant impact not only on the regioselectivity and extent of the HDF reactivity but also on the chemoselectivity through competition with an alternative C−H bond activation process. DFT calculations are used to probe the possible mechanisms of the HDF reactions and explore the competition between C−F and C−H bond activation.[13]

RESULTS

Experimental Studies on the Hydrodefluorination of $C_5F_{5-x}H_x$ (x = 0−2) with Ru(NHC)$(PPh_3)_2(CO)H_2$ (NHC = IPr 1, IMes 2). The most active of the Ru-NHC catalysts, the *N*-diisopropylphenyl substituted species Ru(IPr)$(PPh_3)_2(CO)H_2$ (**1**), was initially employed for the HDF of a range of fluoropyridines with Et_3SiH as the reductant. A summary of the catalytic results is shown in Table 1.

Although HDF of C_5F_5N had previously been reported,[8] this process was reinvestigated as a benchmark for comparison to other substrates. Thus, under a standard set of reaction conditions (28 h reaction at 343 K in THF with 10 mol % loading of **1**), C_5F_5N underwent 90% conversion to a mixture of five products (Entry 1), which were identified on the basis of their ^1H and ^{19}F NMR spectra as lower fluorine-containing species resulting from up to three HDF steps. The major product was 2,3,4,5-C_5F_4HN, formed through activation of the C−F bond *ortho* to the pyridyl nitrogen; taken together with the amounts of 3,4,5-$C_5F_3H_2N$, 2,3,5-$C_5F_3H_2N$ and 3,4-$C_5F_2H_3N$, ca. 80% of the products result from cleavage of an

Scheme 1. Ru-Catalyzed HDF of C_6F_5H to 1,2,3,4-$C_6F_4H_2$

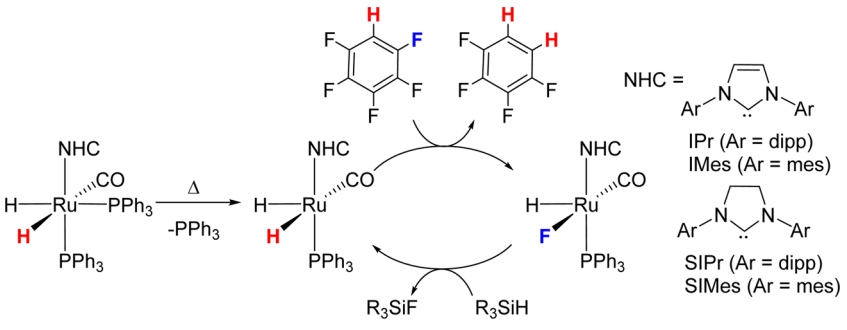

DOI: 10.1021/cs501644r
ACS Catal. 2015, 5, 776−787

Table 1. Product Distribution for the Catalytic HDF of Fluoropyridines by Ru(NHC)(PPh$_3$)$_2$(CO)H$_2$ (NHC = IPr (1), IMes (2))[a]

Entry	[Ru]	Substrate	T(K)	Time	Product distribution (%)[b]							TON[c]
					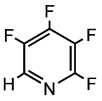	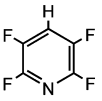	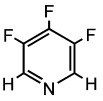	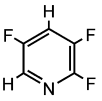	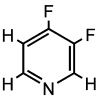	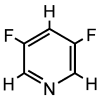	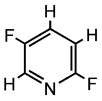	
1	**1**[d]	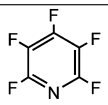	343	28 h	42	22	21	7	3	0	0	13
2	**1**[d]		363	28 h	26	20	41	8	2	0	0	15
3	**1**[d]		343	7 days	21	19	45	12	2	0	0	16
4	**1**	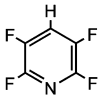	343	28 h	-	96	-	4	-	0	0	<1
5	**1**	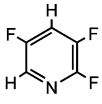	343	28 h	-	-	-	75	-	11	14	3
6	**1**	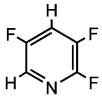	343	3 days	-	-	-	32	-	27	41	8
7	**2**[d]	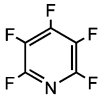	343	28 h	12	40	0	7	0	0	0	6
8	**2**	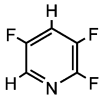	343	28 h	-	-	-	91	-	1	8	1
9	**2**	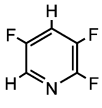	343	3 days	-	-	-	85	-	1	14	2

[a]Conditions: 10 mol % Ru, 0.05 mM substrate, 0.1 mM Et_3SiH, 0.5 mL THF. [b]Determined by integration of the ^{19}F NMR spectra relative to an external standard of α,α,α-trifluorotoluene. Values are the average of three catalytic runs. [c]TON = (moles of fluoroaromatic products × number of HDF steps)/mols of catalyst. [d]Remaining C_5F_5N accounts for the yields being <100%.

ortho C−F bond, supporting the high regioselectivity of the Ru system.

Increasing the temperature to 363 K (Entry 2) or reaction time to 7 days at 343 K (Entry 3) promoted additional HDF. As a result, the percentage of products resulting from more than a single HDF step increased from ca. 30% at 343 K to 51% at 363 K and to 59% with the extended time. In both reactions, 3,4,5-$C_5F_3H_2N$ was the major product as a result of HDF at the second *ortho*-position. Of note is that the modified conditions did not change the amount of 2,3,5,6-C_5F_4HN formed (relative to the standard reaction), indicating that this product is inert to further HDF; indeed, only a minimal amount of HDF was observed when 2,3,5,6-C_5F_4HN was used as the substrate in a catalytic run (Entry 4). ^1H and $^{31}P\{^1H\}$ NMR spectra revealed that **1** was still fully intact (vide infra).

Interestingly, changing the *ortho* N-substituent from F (in 2,3,5,6-C_5F_4HN) to H (in 2,3,5-$C_5F_3H_2N$) resurrected some, albeit modest, HDF activity, producing the difluoropyridines, 3,5-$C_5F_2H_3N$ and 2,5-$C_5F_2H_3N$ (Entries 5 and 6). There was no evidence for further reduction to any mono fluoropyridine products, consistent with the general paucity of catalytic systems in the literature able to react with mono- or difluorinated substrates.[5e]

In agreement with the previous results with C_6F_6 and C_6F_5H,[8] the Ru-IMes complex **2** proved to be a less active catalyst for the HDF of C_5F_5N, giving ca. 60% conversion in 28 h at 343 K (Entry 7). Moreover, there was now a switch in the regioselectivity of the reaction, with the *para*-HDF product 2,3,5,6-C_5F_4HN present as the major component of the products. In this case, attempts to bring about HDF of 2,3,5,6-C_5F_4HN itself resulted instead in the loss of catalyst **2** through competitive C−H activation to afford the fluoropyridyl hydride complex, Ru(IMes)(PPh$_3$)(CO)(4-C_5F_4N)H (**3**). This pathway helps to account for the poorer catalytic activity of **2** toward C_5F_5N, as the catalyst is shunted off the catalytic cycle by C−H activation of the initial product of HDF. Interestingly,

DOI: 10.1021/cs501644r
ACS Catal. 2015, 5, 776−787

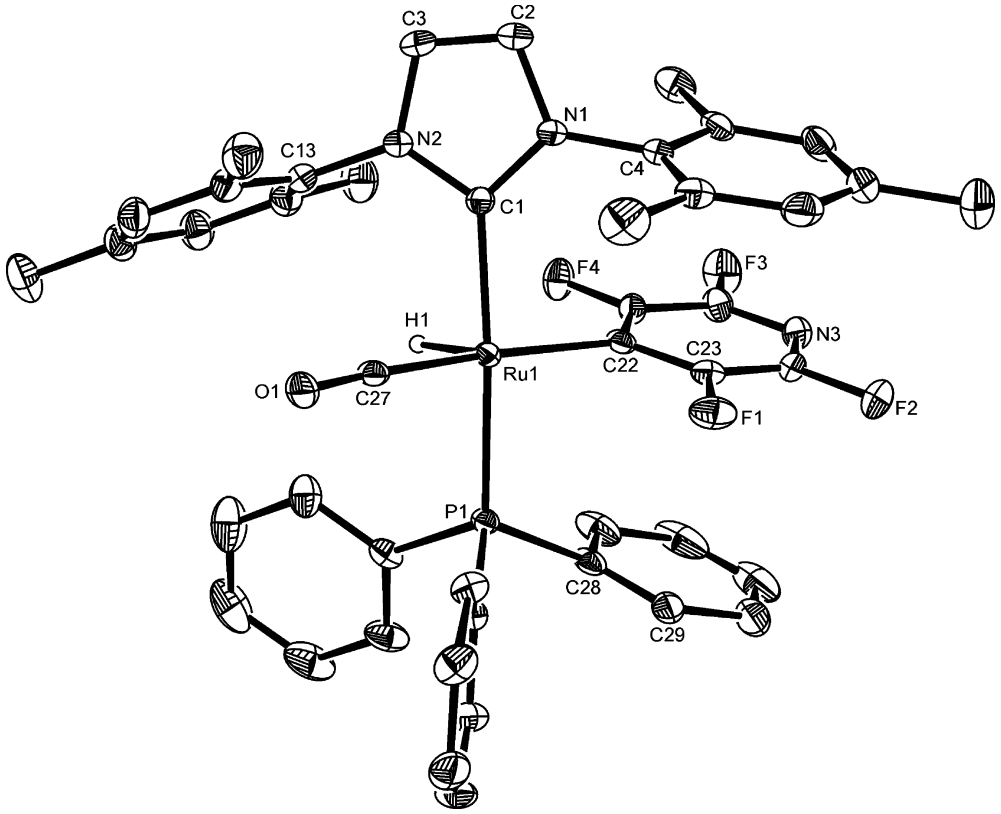

Figure 1. X-ray crystal structure of Ru(IMes)(PPh_3)(CO)(4-C_5F_4N)H (**3**). Ellipsoids shown at 30% level with all hydrogen atoms (except Ru−H) omitted for clarity. Selected bond lengths (Å) and angles (deg): Ru(1)−C(1) 2.106(2), Ru(1)−C(22) 2.148(2), Ru(1)−C(27) 1.862(2), Ru(1)−P(1) 2.3468(6), C(1)−Ru(1)−P(1) 174.06(7), C(22)−Ru(1)−C(27) 174.27(10), C(1)−Ru(1)−C(22) 91.07(7).

Scheme 3. Possible Mechanisms for Catalytic HDF of C_5F_5N at 1 and 2 To Give 2,3,4,5-C_5F_4HN[a]

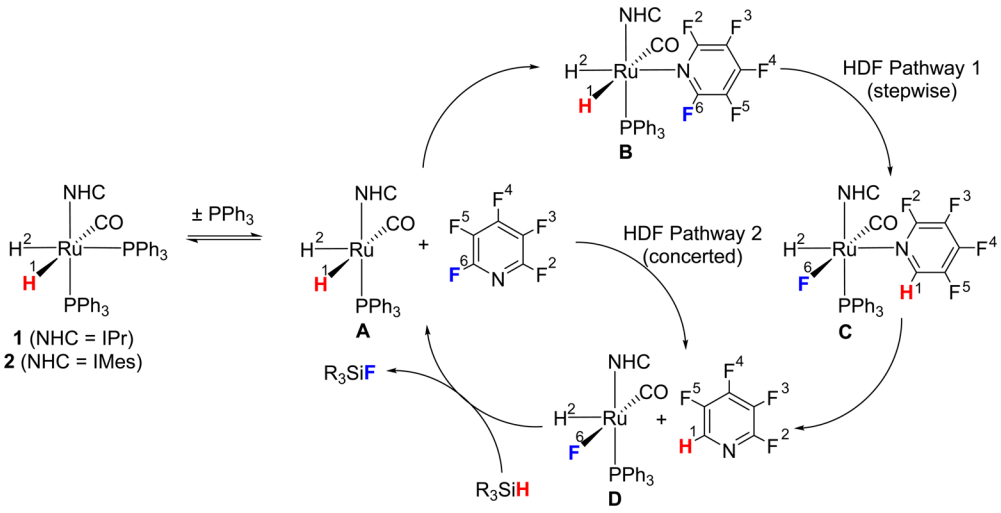

[a]The numbering scheme used in the text is also shown for those atoms involved in the HDF reaction, where ring carbons take the same number as their F-substituent in C_5F_5N.

C−H cleavage was not observed when 2,3,5,6-C_5F_4HN was changed to 2,3,5-$C_5F_3H_2N$, although only very low HDF activity was recorded, even with prolonged reaction times (Entries 8 and 9).

Isolation and Characterization of Ru(IMes)(PPh_3)(CO)-(4-C_5F_4N)H (3). Complex **3** was fully characterized by multinuclear NMR spectroscopy and X-ray crystallography following isolation as dark orange crystals from a stoichiometric reaction of **2** with 2,3,5,6-C_5F_4HN at 323 K for 4 days. The X-ray crystal structure (Figure 1) displayed the anticipated square-based pyramidal structure with an apical hydride ligand. π-Stacking in the molecule is evidenced by a centroid-centroid distance of 3.52 Å between the aromatic rings based on C4 and C22 and the comparatively smaller distance of 3.40 Å between the fluoropyridyl ring and the phenyl group based on C28. The associated angles between the mean-planes of pairs of adjacent rings are 4.3° (rings based on C4 and C22) and 10.2° (rings based on C22 and C28), respectively. The achievement of the

DOI: 10.1021/cs501644r
ACS Catal. 2015, 5, 776−787

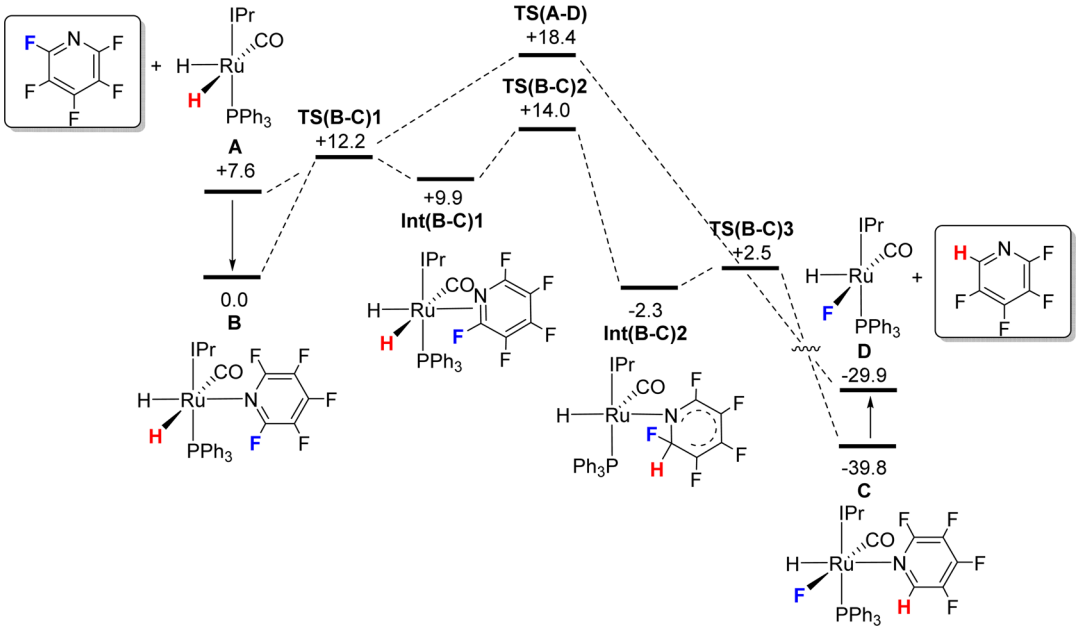

Figure 2. Computed Free Energy Profiles (BP86-D3(THF), kcal/mol) for HDF of C_5F_5N following PPh_3 loss at **1** to give 2,3,4,5-C_5F_4HN via either stepwise Pathway 1 (via **B**) or concerted Pathway 2 (direct from **A**).

latter occurs concomitantly with substantial deviation in the phosphine ligand, such that the P1−C28−C29-C30 angle has a value of 165.6° rather than an ideal value of 180°. The Ru−$C_{fluoroaryl}$ distance is comparable to that found in the related coordinatively saturated analogue, Ru(ICy)(dppp)(CO)(4-C_5F_4N)H (ICy = 1,3-dicyclohexylimidazol-2-ylidene; dppp =1,4-bis(diphenylphosphino)propane).[14]

The solution NMR data were consistent with the solid-state structure. The low frequency (δ −26.2) of the Ru−H resonance was indicative of a vacant *trans*-coordination site, while the doublet of doublet of doublets multiplicity resulted from the expected *cis*-^{31}P coupling, along with coupling to the two *ortho*-fluorines of the static C_5F_4N ligand. This lack of free rotation about the Ru−$C_{fluoroaryl}$ bond led to the appearance of four separate ^{19}F signals at δ −103, −105, −116, and −124. The two lowest frequency signals were assigned to those *ortho* to the Ru-bound carbon atom on the basis of ^{1}H−^{19}F HOESY and HMBC spectroscopy (Supporting Information).

Computational Studies. DFT calculations were undertaken to establish the mechanism of fluoropyridine HDF by **1** and **2** and to probe the factors controlling the different chemo- and regioselectivities observed with these two catalyst precursors. The calculations here employed the full experimental structures, as previous studies have shown the importance of the NHC ligand architecture in both promoting HDF and dictating the selectivity of that process.[10,11] We report free energies calculated with the BP86 functional in the gas-phase and then corrected for both THF solvent (PCM approach) and dispersion effects (Grimme's D3 parameter set) via single point energy calculations at the BP86-optimized geometries (see Computational Details).

A general HDF catalytic cycle is shown in Scheme 3, based on the reaction of C_5F_5N at the *ortho* position to give 2,3,4,5-C_5F_4HN. Starting from the 6-coordinate precursors (**1** or **2**) catalysis is initiated by loss of PPh_3 to give the 16e dihydride intermediate **A**. Calculations showed PPh_3 dissociation to be *ca.* 14 kcal/mol more accessible when *trans* to hydride than when *trans* to the NHC; this was also borne out experimentally by exchange reactions with PPh_3-d_{15} (see Figures S11 and S12, Supporting Information). Moreover, the isomer formed in the latter process readily rearranges with a minimal barrier of around 3 kcal/mol to give the lower energy form with an axial hydride. As with our previous studies on fluoroarenes,[10,11] two pathways for the HDF step have been characterized from Intermediate **A**. In Pathway 1, HDF proceeds in a stepwise, intramolecular fashion via the N-bound C_5F_5N complex **B**[15] and leads to an analogous adduct of the 2,3,4,5-C_5F_4HN product, **C**. Dissociation then gives 16e Ru hydride fluoride **D**, which can react with trialkylsilanes to regenerate the active dihydride **A**. In Pathway 2, HDF is a concerted process in which 16e **A** reacts with C_5F_5N in an intermolecular fashion to generate the HDF product and hydride fluoride species **D** directly in one step.

Reactions of C_5F_5N at 1. We consider first the details of these two pathways for the HDF of C_5F_5N at **1**, for which reaction at the *ortho* position is preferred experimentally. In the following, all free energies are quoted relative to the N-bound C_5F_5N adduct **B**, which is set to zero. The computed free energy profiles for HDF of C_5F_5N at the *ortho* position via Pathways 1 (stepwise) and 2 (concerted) are compared in Figure 2, with key computed structures shown in Figure 3. The first step along Pathway 1 is C_5F_5N addition to **A** to give adduct **B** with a computed binding free energy of 7.6 kcal/mol.[16] **B** is most stable as this N-bound form and exhibits a Ru−N distance of 2.30 Å. The most accessible alternative π-bound isomer is 3.1 kcal/mol higher in energy than **B** and binds through the C^3═C^4 bond. This preference contrasts that observed experimentally[17] or in calculations[18] on Group 10 M$(PR_3)_2(C_5F_5N)$ species where a π-bound form is preferred, and this probably reflects the greater π-basicity of the bent {M$(PR_3)_2$} fragments in those studies. A few N-bound adducts of C_5F_5N have been structurally characterized experimentally, with the most relevant here being *cis*-[Re(P^iPr_3)$(CO)_4(NC_5F_5)$][BAr^F_4] (Ar^F = 3,5-$C_6H_3(CF_3)_2$) where the Re−N distance is 2.319(5) Å.[19] Several square-planar Pt(II) σ-adducts are also known,[20] but none to date are known for Ru.

DOI: 10.1021/cs501644r
ACS Catal. 2015, 5, 776−787

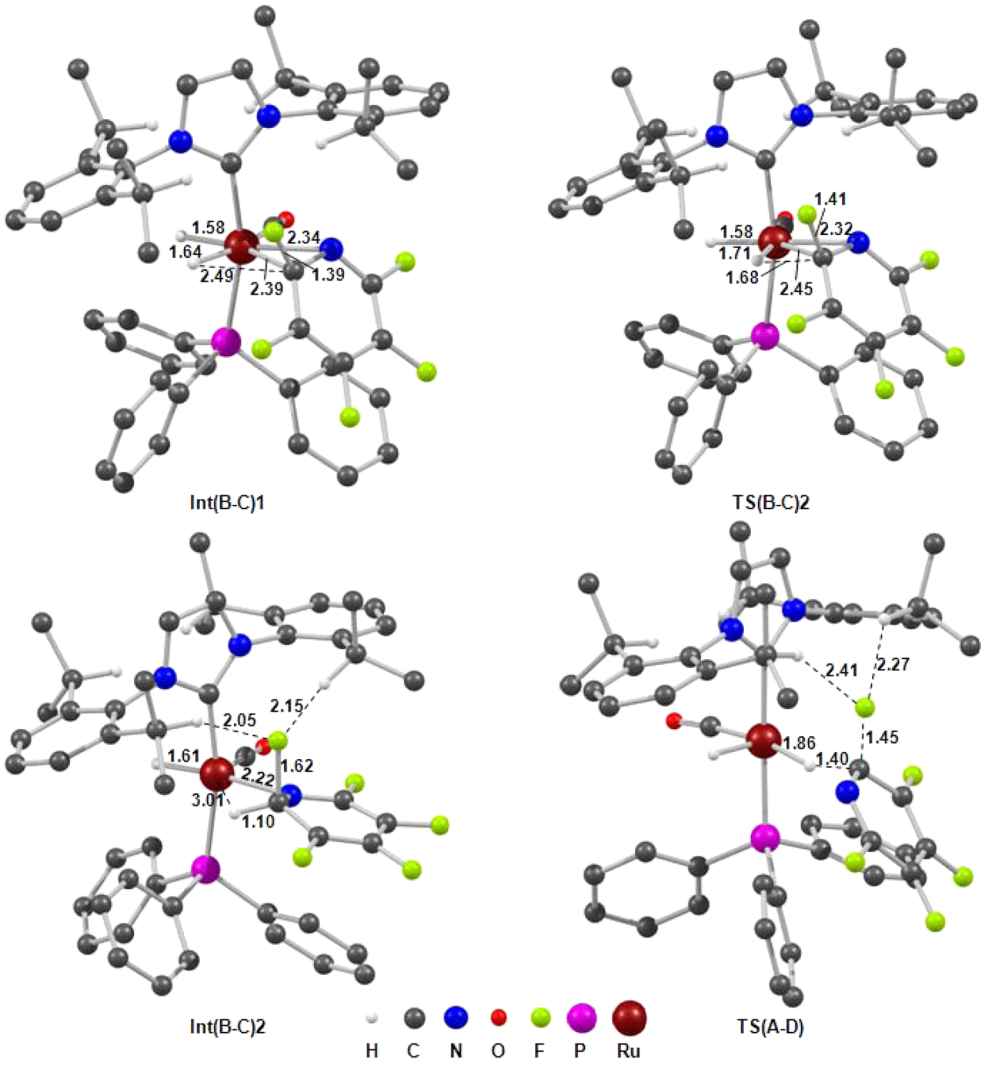

Figure 3. Computed structures of **Int(B−C)1**, **TS(B−C)2**, **Int(B−C)2** (Pathway 1) and **TS(A-D)** (Pathway 2) with key distances in Å. H atoms, with the exception of IPr methine and participating hydride ligands, are omitted for clarity.

Stepwise HDF along Pathway 1 proceeds through an initial isomerization of **B** via **TS(B−C)1** (G = +12.2 kcal/mol) to give a $\pi_{(C,N)}$-bound intermediate, **Int(B−C)1** (G = +9.9 kcal/mol: Ru−N = 2.34 Å; Ru−C^6 = 2.39 Å). The geometry of **Int(B−C)1** is set up for attack of H^1 at the ring C^6 position and this proceeds via **TS(B−C)2** (G = +14.0 kcal/mol) with transfer of H^1 from Ru onto C^6 (Ru···H^1 = 1.71 Å; C^6···H^1 = 1.68 Å), and elongation of the Ru−C^6 and C^6−F^6 bonds to 2.45 and 1.41 Å, respectively. The Ru−N distance is not much altered at this point (2.32 Å), but it subsequently shortens significantly to 2.22 Å in **Int(B−C)2** (G = −2.3 kcal/mol), which also features an intact C^6−H^1 bond (1.10 Å) and further elongation of the C^6−F^6 distance (1.62 Å). The {C_5F_5HN} moiety in **Int(B−C)2** therefore resembles a Meisenheimer intermediate formed by the intramolecular nucleophilic (S_NAr) attack of hydride. Consistent with this picture is the lengthening of both the C^6−C^5 and C^6−N distances to 1.45 and 1.40 Å, respectively (cf. 1.40 and 1.33 Å in free C_5F_5N), while the short Ru−N distance suggests significant stabilization via N → Ru σ-donation. **Int(B−C)2** represents a relatively late point on the S_NAr coordinate, as evidenced by the long C^6−F^6 distance and the increased NBO negative charge on F^6 (−0.46 cf. an average charge of −0.31 on the remaining ring fluorines). This fluoridic character also leads to short (<2.2 Å) F^6···H−C contacts to two methine hydrogens on the IPr isopropyl substituents. Similar stabilizing interactions were noted in our previous study on HDF of C_6F_5H and were important in directing the *ortho* selectivity of that process.[10,11] The onward reaction of **Int(B−C)2** involves the facile cleavage of the weakened C^6−F^6 bond via **TS(B−C)3** (G = +2.5 kcal/mol: C^6···F^6 = 1.79 Å; Ru···F^6 = 3.29 Å), with F-transfer to Ru to give **C**, the N-bound adduct of 2,3,4,5-C_5F_4HN (G = -39.8 kcal/mol). This contrasts with the computed mechanism with C_6F_5H where HF is formed at this stage,[10,11] and possibly reflects the much shorter C^6−H^1 bond in the present case which being essentially fully formed is resistant to deprotonation. From **C** the catalytic cycle would be completed by dissociation of 2,3,4,5-C_5F_4HN to give 16e **D** (G = −29.9 kcal/mol) followed by reduction with Et_3Si−H to regenerate **A**. The barrier for the latter process has been calculated to be 11.1 kcal/mol.

Along Pathway 2 the hydride ligand *trans* to CO in **A** attacks C_5F_5N directly without any prior coordination of the fluoroaromatic. The HDF proceeds in one step via **TS(A-D)** (G = +18.4 kcal/mol) in which the Ru···H^1 distance has lengthened to 1.86 Å and the C^6−H^1 bond is beginning to form (C^6···H^1 = 1.40 Å). This promotes a lengthening of the C^6−F^6

DOI: 10.1021/cs501644r
ACS Catal. 2015, 5, 776−787

Table 2. Computed Free Energies (kcal/mol) of Key Stationary Points Associated with HDF at the *ortho*, *meta* and *para* Positions of C_5F_5N via Pathways 1 and 2 at Catalysts 1 (NHC = IPr) and 2 (NHC = IMes)[a]

pathway	1 (stepwise)				2 (concerted)
catalyst **1**	**Int(B−C)1**	**TS(B−C)2**	**Int(B−C)2**	**TS(B−C)3**	**TS(A-D)**
ortho	+9.9	+14.0	−2.3	+2.5	+18.4
meta	+5.3	+16.2	+14.6	+19.0	+18.7
para	+3.1	+11.2	+8.8	+16.6	+16.1
catalyst **2**	**Int(B−C)1**	**TS(B−C)2**	**Int(B−C)2**	**TS(B−C)3**	**TS(A-D)**
ortho	+12.5	+16.8	+2.5	+3.1	+20.2
meta	+7.2	+17.7	+15.8 → +6.8[b]	+16.9	+19.3
para	+6.8	+14.5	+12.7 → −0.3[b]	+17.2	+15.9

[a]All energies are quoted relative to adduct **B** at 0.0 kcal/mol for each system. [b]Alternative forms of **Int(B−C)2** are implicated in the reaction profile: see text for details.

bond to 1.45 Å and, as this lies parallel to the Ru−NHC bond, this also permits two short $F^6\cdots H-C$ contacts (2.41 and 2.27 Å) to develop to the IPr ligand which may further promote this process.[21] **TS(A-D)** leads directly to 16e **D** and free 2,3,4,5-C_5F_4HN. Of the two possible mechanisms considered for the *ortho* HDF of C_5F_5N at **1**, stepwise Pathway 1 proceeds with a lower overall barrier of 14.0 kcal/mol, and therefore, this is clearly favored kinetically over concerted Pathway 2, which has an overall barrier of 18.4 kcal/mol.

To assess the overall regioselectivity of C_5F_5N HDF at **1**, the reactions at the *meta* and *para* positions were also considered via both Pathways 1 and 2. Table 2 displays the computed free energies (relative to the N-bound adduct **B**) of the key stationary points for these processes, alongside those already discussed for HDF at the *ortho* position. For Pathway 2 very similar geometries were located for **TS(A-D)** to that seen above for *ortho* activation. Barriers indicate this pathway is slightly higher for the *meta* position (18.7 kcal/mol) but somewhat more accessible for the *para* position (16.1 kcal/mol).[22] Along Pathway 1, the energy of **TS(B−C)2** follows the same trend, and in each case, this transition state is computed to be lower in energy than **TS(A-D)**. This pattern of reactivity (*para* > *ortho* > *meta*) is consistent with a nucleophilic attack mechanism and is also seen in the S_NAr reactions of free C_5F_5N with simple alkoxide nucleophiles.[23] For *ortho* HDF along Pathway 1 **TS(B−C)2** is higher than the subsequent F-transfer transition state **TS(B−C)3** and so **TS(B−C)2** is rate-determining. However, this is no longer the case for HDF at the *meta* and *para* positions as now both **Int(B−C)2** and **TS(B−C)3** are significantly destabilized, reflecting the fact that no N → Ru stabilization is possible when HDF occurs at the remote *meta* and *para* positions. As a result **TS(B−C)3** becomes the rate-limiting transition state for HDF at the *meta* and *para* positions via Pathway 1. This situation is similar to that seen previously for the HDF of C_6F_5H, where the C−F bond cleavage step along Pathway 1 (equivalent to **TS(B−C)3** here) was rate-limiting for all three *ortho*-, *meta*-, and *para*-HDF reactions.[24] The destabilization of **TS(B−C)3** for *meta* and *para* HDF along Pathway 1 moves these above **TS(A-D)** computed for Pathway 2. The concerted pathway is therefore favored for these reactions, although as the difference in energy between the rate-limiting transition states is very small (<0.5 kcal/mol), one might expect both pathways to be operative.

For the reaction of C_5F_5N at **1**, the overall computed order of reactivity is for HDF to occur at the *ortho* position (via Pathway 1, $\Delta G^{\ddagger}$ = +14.0 kcal/mol) in preference to reaction at the *para* position (via Pathway 2, $\Delta G^{\ddagger}$ =+16.1 kcal/mol) with reaction at the *meta* position least likely (via Pathway 2, $\Delta G^{\ddagger}$ = +18.7 kcal/mol). This qualitatively reproduces the experimental observations where *ortho*-HDF dominates with minor products arising from *para*-HDF (Table 1, Entries 1−3).

Table 2 also includes the equivalent data for HDF of C_5F_5N using the IMes-based catalyst **2**. *ortho*-HDF proceeds in a similar fashion to that seen for **1**, however for *meta*- and *para*-HDF a more stable form of **Int(B−C)2** is implicated in the reaction. This new species, **Int(B−C)2′**, lies at +6.8 kcal/mol and −0.3 kcal/mol for *meta*- and *para*-HDF, respectively, and differs from **Int(B−C)2** by a rotation of the {C_5F_5HN} moiety which allows the C−F bond adjacent to the sp^3 carbon to lie parallel to the Ru−IMes bond. IRC calculations show that for the Ru-IMes system **Int(B−C)2′** links directly to **TS(B−C)3**; see Figure S20 in the Supporting Information.[25] This additional feature does not, however, affect the overall barriers to HDF at **2** as *para*-HDF is favored through **TS(A-D)** at +15.9 kcal/mol, while the rate-limiting transition state for *meta*-HDF is **TS(B−C)2** at +17.7 kcal/mol.

Comparing the HDF profiles in Table 2 shows the energies of both **Int(B−C)1** and **TS(B−C)2** to be 2−4 kcal/mol higher for all three HDF processes when computed with the Ru-IMes system **2**. **TS(A-D)** is also destabilized for *ortho* and *meta* HDF, although the effect here is smaller. Most significantly a change in *ortho*/*para* selectivity is seen, the most accessible reaction at **2** being HDF at the *para* position (via Pathway 2, $\Delta G^{\ddagger}$ = +15.9 kcal/mol), followed by reaction at the *ortho* position (via Pathway 1, $\Delta G^{\ddagger}$ = +16.8 kcal/mol) with the *meta* position again least favored (via Pathway 1, $\Delta G^{\ddagger}$ = +17.7 kcal/mol). These changes are consistent with 2,3,5,6-C_5F_4HN being the dominant HDF product formed with **2**, with smaller amounts of products (2,3,4,5-C_5F_4HN and 2,3,5-$C_5F_3H_2N$) arising from *ortho*-HDF being seen (see Table 1, Entry 7). The switch in mechanism appears to be related to the greater accessibility of **Int(B−C)1** when formed with the IPr catalyst **1**, which is then carried through to give a lower energy for **TS(B−C)2** in this case.

HDF of Lower Fluorinated Substrates at 1. With Ru-IPr catalyst **1**, the major initial product, 2,3,4,5-C_5F_4HN, can undergo further HDF to give 3,4,5-$C_5F_3H_2N$ and 2,3,5-$C_5F_3H_2N$. 3,4-$C_5F_2H_3N$ is also seen in trace amounts in these initial runs, and this can only originate from 3,4,5-$C_5F_3H_2N$ (see Table 1 Entries 1−3). No HDF products derived from 2,3,5-$C_5F_3H_2N$ are apparent, possibly as this species is only formed in relatively small amounts. Indeed, if 2,3,5-$C_5F_3H_2N$ is introduced in a separate run as the sole substrate then formation of the HDF products 3,5-$C_5F_2H_3N$ and 2,5-$C_5F_2H_3N$ is seen (see Entries 5 and 6). In general, HDF becomes more difficult as the number of F-substituents

DOI: 10.1021/cs501644r
ACS Catal. 2015, 5, 776−787

decreases, thus no evidence for HDF of either isomer of $C_5F_2H_3N$ is seen under the present conditions.

We have computed reaction profiles for these various HDF processes, and the energies of the relevant rate-limiting transition states along both Pathways 1 and 2 are reported in Figure 4. For a given position, the computed HDF barrier

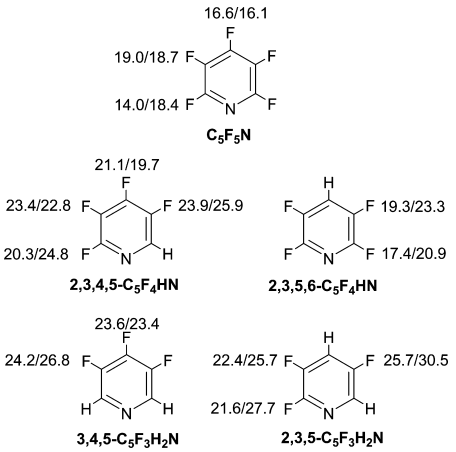

Figure 4. Free energies (kcal/mol) of rate-limiting transition states for the HDF of fluoropyridines $C_5F_{5-x}H_xN$ (x = 0−2) at catalyst **1**. Two values corresponding to Pathway 1/Pathway 2 are shown for each unique C−F bond, and all energies are quoted relative to the relevant N-bound precursor adduct **B** at 0.0 kcal/mol. Only isomers implicated in the experimental studies are shown.

increases as the numbers of F substituents elsewhere in the aromatic ring are reduced. Thus, the low barriers for *ortho* and *para* HDF of C_5F_5N (14.0 and 16.1 kcal/mol, respectively) increase to +20.3 kcal/mol and +19.7 kcal/mol for the equivalent processes with 2,3,4,5-C_5F_4HN. *para*-HDF in 3,4,5-$C_5F_3H_2N$ then has a further increased barrier of 23.4 kcal/mol, while *para*-HDF in 3,4-$C_5F_2H_3N$ has a slightly higher barrier of 23.7 kcal/mol.

The similar computed barriers of around 20 kcal/mol for *ortho*- and *para*-HDF of 2,3,4,5-C_5F_4HN are consistent with the mixture of 3,4,5-$C_5F_3H_2N$ and 2,3,5-$C_5F_4H_2N$ seen experimentally, although the calculations do suggest somewhat more of the 2,3,5-$C_5F_3H_2N$ isomer might be formed than is seen experimentally. In this case, HDF at the two distinct *meta* C−F bonds of 2,3,4,5-C_5F_4HN cannot compete due to transition states above +22 kcal/mol, and the corresponding products are not observed experimentally. For 2,3,5-$C_5F_3H_2N$, transition states at +21.6 and 22.4 kcal/mol would permit reaction at the 2- and 3-positions to form the observed 3,5- and 2,5-isomers of $C_5F_2H_3N$ respectively (Table 1, Entries 5 and 6). HDF of 3,4,5-$C_5F_3H_2$ has transition states at +24.2 kcal/mol and +23.4 kcal/mol for the *meta*- and *para*- positions respectively; thus, despite 3,4,5-$C_5F_3H_2$ being formed in reasonable amounts (Table 1, Entries 1−3), subsequent prolonged heating only results in trace amounts of the 3,4-isomer of $C_5F_2H_3N$ being seen. Overall, the calculations provide a reasonable qualitative description of the relative reactivities of the different fluoropyridines, in particular the decreased HDF activity as the number of F-substituents is reduced. The calculations also correctly identify the most likely sites for HDF, although here the computed barriers do not always reflect the precise product distributions seen experimentally.

In contrast, the computational modeling of the lower reactivity of the 2,3,5,6-C_5F_4HN isomer has been less successful. This species is formed as a minor HDF product of C_5F_5N with **1** and, compared to the 2,3,4,5-C_5F_4HN isomer, is far more reluctant to undergo any further HDF reactions, despite both fluoropyridines having four remaining F-substituents (Table 1, Entry 4). HDF of 2,3,5,6-C_5F_4HN is computed to have rate-limiting transition states at 17.4 and 19.3 kcal/mol for the *ortho*- and *meta*-positions, respectively. Although these indicate a significantly lower reactivity than C_5F_5N, these barriers are both lower than the most accessible HDF transition state of the 2,3,4,5-isomer (20.3 kcal/mol), predicting that 2,3,5,6-C_5F_4HN should be amenable to HDF, in contrast to what is observed experimentally. Instead, 2,3,5,6-C_5F_4HN yields only trace amounts of the *ortho* HDF product under standard conditions (Table 1, Entry 4). The accessibility of HDF in 2,3,5,6-C_5F_4HN is therefore overestimated in the current approach (see Discussion below).

C−H Bond Activation of 2,3,5,6-C_5F_4HN at 2. HDF of C_5F_5N by Ru-IMes catalyst **2** leads to 2,3,5,6-C_5F_4HN and the calculations indicate this change in regioselectivity (compared to catalyst **1**) arises as Pathway 2 is operative and directs HDF to the *para* position (see Table 2). In further contrast to the situation with **1**, the IMes system then reacts further with 2,3,5,6-C_5F_4HN to give the C−H activated product **3**. The computed mechanism for this process is shown in Figure 5 and

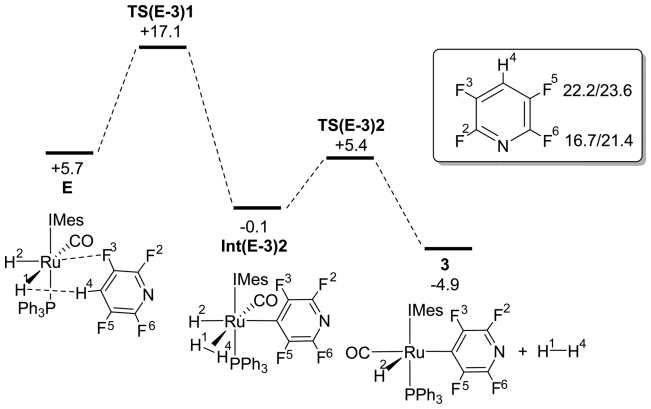

Figure 5. Computed free energy profile (BP86-D3(THF), kcal/mol) for C−H activation of 2,3,5,6-C_5F_4HN following PPh_3 loss at **2** to give **3**. The inset provides barriers for the competing barriers to HDF via Pathway 1/Pathway 2. All energies are relative to the N-bound adduct of 2,3,5,6-C_5F_4HN set to 0.0 kcal/mol. The numbering of key atoms is also shown, where ring carbons take the same number as their substituent in 2,3,5,6-C_5F_4HN.

proceeds from precursor **E** (G = +5.7 kcal/mol), a non-covalently bound adduct featuring a weak Ru···F^3 interaction (2.82 Å) and a Ru−H^1···H^4−C^4 dihydrogen interaction (2.10 Å). C^4−H^4 bond activation then proceeds through **TS(E-3)1** (see also Figure 6) with transfer of H^4 onto H^1 and concomitant Ru−C^4 bond formation to give dihydrogen complex **Int(E-3)2** at −0.1 kcal/mol. Dissociation of H_2 is then coupled with isomerization of the coordination geometry at Ru such that the remaining hydride, H^2, moves into an axial site, *trans* to the vacant site in the resultant square-pyramidal product **3** (G = −4.9 kcal/mol). C−H activation is therefore exergonic relative to the N-bound adduct of 2,3,5,6-C_5F_4HN and proceeds with an overall barrier of 17.1 kcal/mol. A further consideration, however, is the competition with any potential

DOI: 10.1021/cs501644r
ACS Catal. 2015, 5, 776−787

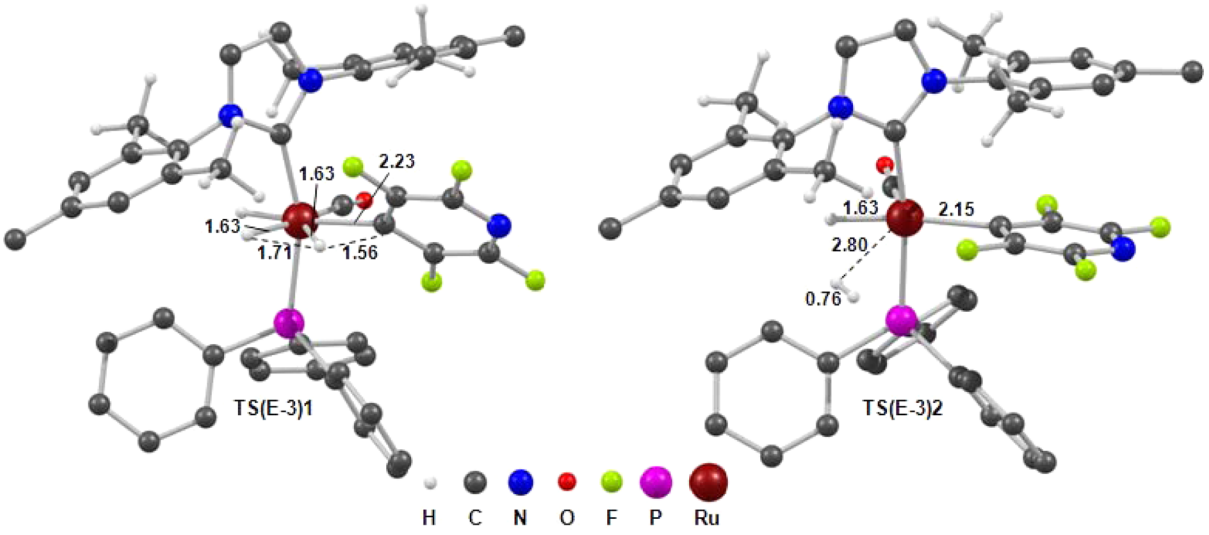

Figure 6. Computed structures of **TS(E-3)1** and **TS(E-3)2** with key distances in Å. PPh_3 and IMes H atoms (with the exception of the IMes *ortho*-Me groups) are omitted for clarity.

HDF processes. These were therefore also computed (see inset, Figure 5) and predict an HDF barrier at the *ortho*-position of only 16.7 kcal/mol, indicating this process should be competitive with C−H activation. Experimentally HDF does not occur to any significant extent in this system and so it again appears that the HDF reactivity of 2,3,5,6-C_5F_4HN is being overestimated in the present calculations.

DISCUSSION

Catalytic HDF reactions of C_5F_5N have been explored both experimentally and computationally with the Ru-IPr and Ru-IMes catalysts **1** and **2**. Experimentally HDF proceeds quite differently with these two species. With **1** HDF is favored at the *ortho*-position to give 2,3,4,5-C_5F_4HN which can undergo further HDF to 3,4,5-$C_5F_3H_2N$ and 2,3,5-$C_5F_3H_2N$. Isolated 2,3,5-$C_5F_3H_2N$ was also shown to undergo HDF to give 3,5-$C_5F_2H_3N$ and 2,5-$C_5F_2H_3N$. The initial HDF of C_5F_5N also gives 2,3,5,6-C_5F_4HN as a minor product, but this species is then inert to any further reaction. In contrast with **2**, HDF of C_5F_5N is favored at the *para*-position and gives 2,3,5,6-C_5F_4HN as the major product. This, however, then undergoes C−H activation to produce fluoropyridyl complex **3** which, being inactive as an HDF catalyst, shuts down any further reactivity.

DFT calculations have defined two possible mechanisms for these HDF reactions based on nucleophilic attack by a hydride ligand in either a stepwise process (Pathway 1) or a concerted process (Pathway 2). Pathway 1 involves a π-bound substrate and favors *ortho*-HDF as this is stabilized by a direct N → Ru interaction in the key C−F bond cleavage transition state. Pathway 2 more resembles a conventional S_NAr process and so favors reaction at the *para*-position. A change in the preferred pathway between catalysts **1** (Pathway 1) and **2** (Pathway 2) captures the different regioselectivities seen experimentally with C_5F_5N, despite the relatively subtle change of NHC from IPr to IMes. This change in the preferred mechanism appears to be linked to the stronger binding of the π-bound intermediate, **Int(B−C)1**, when formed with **1**. Further calculations on the reactivity of the IPr system reproduced the trends seen in the subsequent HDF reactions of 2,3,4,5-C_5F_4HN, and correctly identified the most likely sites for the two subsequent HDF steps that give isomers of $C_5F_3H_2N$ and $C_5F_2H_3N$. In most cases, experiment and calculations showed two alternative HDF processes to be in close competition, and the precise product distributions were not always correctly modeled in the calculations. However, the differences in energy that are reflected in these product distributions are small and do not represent a significant absolute error in the calculations.

A more significant issue is the apparent difficulty in modeling the reactivity of 2,3,5,6-C_5F_4HN, which the calculations indicate should be amenable to further HDF with both catalysts **1** and **2**. We therefore considered (i) the functional-dependency of our results and (ii) whether an alternative mechanism may be in play. To address point (i) we first recomputed the energies of the most accessible HDF transition states of 2,3,4,5-C_5F_4HN and 2,3,5,6-C_5F_4HN at IPr catalyst **1** with a range of different functionals: BP86, BLYP, B3LYP, PBE, PBE0 (both with and without a dispersion correction); M06, M06L; B97D, B97D3 and ωB97xD, giving a total of 15 different approaches (see Table S2 in the Supporting Information). With our standard BP86-D3(THF) protocol these HDF transition states are at +20.3 kcal/mol and +17.4 kcal/mol, respectively, a difference of 2.9 kcal/mol indicating (incorrectly) a preference for HDF at 2,3,5,6-C_5F_4HN. This preference, however, is remarkably consistent across all 15 computational methods, ranging from 4.2 to 2.5 kcal/mol. Similarly, we reassessed the difference between C−H activation and HDF of 2,3,5,6-C_5F_4HN at catalyst **2**. In this case the BP86-D3(THF) protocol gave barriers of 17.1 and 16.7 kcal/mol, respectively, favoring HDF by 0.4 kcal/mol; this preference was again reproduced by the other 15 methods tested. Our results are therefore not functional dependent.

To address point (ii), the possibility of an alternative mechanism, we considered the initial oxidative addition of C_5F_5N to form a Ru(IV) fluoropyridyl intermediate Ru(NHC)-$(PPh_3)(CO)(F)(H)_2(C_5F_4N)$. This was done for NHC = IPr and gave barriers of 26.8 and 22.3 kcal/mol for activation at the *ortho*- and *para*-positions, respectively. These values rule out oxidative addition as a viable process, being between 6 to 12 kcal/mol higher than the most accessible hydride attack transition states (as well as predicting a *para*-selectivity not seen experimentally). At present, we are therefore unable to account for the anomalous results obtained in modeling the

DOI: 10.1021/cs501644r
ACS Catal. 2015, 5, 776−787

reactivity of 2,3,5,6-C_5F_4HN at these $Ru(NHC)(PPh_3)_2(CO)(H)_2$ catalysts, and the reasons for this will be the subject of future work.

CONCLUSIONS

We have reported here a joint experimental and computational study of the catalytic hydrodefluorination (HDF) reactions of C_5F_5N at $Ru(NHC)(PPh_3)_2(CO)H_2$, where NHC = IPr (**1**) or IMes (**2**). The observed reactivity is highly dependent on the NHC ligand. With catalyst **1**, HDF occurs preferentially at the *ortho*-position to give 2,3,4,5-C_5F_4HN, while *para*-HDF forms 2,3,5,6-C_5F_4HN as a minor product. 2,3,4,5-C_5F_4HN can then undergo further HDF to 3,4,5-$C_5F_3H_2N$ and 2,3,5-$C_5F_3H_2N$. Isolated 2,3,5-$C_5F_3H_2N$ also undergoes HDF to give 3,5-$C_5F_2H_3N$ and 2,5-$C_5F_2H_3N$. In contrast, 2,3,5,6-C_5F_4HN does not undergo any further reaction. With catalyst **2**, HDF of C_5F_5N is favored at the *para*-position and gives 2,3,5,6-C_5F_4HN as the major product. In this case 2,3,5,6-C_5F_4HN undergoes C−H activation to produce fluoropyridyl complex **3.** As **3** is not an active HDF catalyst, its formation severely curtails the overall HDF activity of catalyst **2**.

The different selectivities of the HDF reactions of C_5F_5N at **1** and **2** are explained by the DFT calculations in terms of a competition between two different pathways, both based on nucleophilic attack by a hydride ligand. With **1**, a stepwise process is operative that proceeds through a π-bound intermediate and favors *ortho*-HDF as this is stabilized by a direct N → Ru interaction in the key C−F bond cleavage transition state. With **2**, a concerted process is more accessible and favors *para*-HDF, similar to a conventional S_NAr process. The calculations give increased (but accessible) barriers for the subsequent HDF reactions to give isomers of $C_5F_3H_2N$ and $C_5F_2H_3N$ and also correctly identify the most reactive C−F bonds. The calculations systematically overestimate the HDF reactivity of 2,3,5,6-C_5F_4HN at both catalyst **1** (where no HDF reaction is seen experimentally) and at catalyst **2** (where C−H activation occurs preferentially).

EXPERIMENTAL SECTION

All manipulations were carried out using standard Schlenk, high vacuum and glovebox techniques using dried and degassed solvents, unless otherwise stated. NMR spectra were recorded on Bruker Avance 400 and 500 MHz NMR spectrometers and referenced to residual solvent signals for ^1H and ^{13}C spectra for C_6D_6 (δ 7.15, 128.0), THF-d_8 (δ 3.58, 25.4) and toluene-d_8 (δ 2.09). $^{31}P\{^1H\}$ and ^{19}F spectra were referenced externally to 85% H_3PO_4 (85%) and $CFCl_3$, respectively (both δ = 0.0). Elemental analysis was performed by the Elemental Analysis Service, London Metropolitan University, London, U.K. Complexes **1** and **2** were prepared according to the literature.[8]

$Ru(IMes)(PPh_3)(CO)(C_5F_4N)H$ (3). A THF (5 mL) solution of $Ru(IMes)(PPh_3)_2(CO)H_2$ (0.070 g, 0.07 mmol) and 2,3,5,6-C_5F_4HN (15 μL, 0.14 mmol) was heated to 323 K for 4 days. After cooling to room temperature, the solvent was removed in vacuo to give an orange solid, which was washed with hexane (3 × 5 mL) and then recrystallized from THF/hexane to give dark orange crystals of **3**. Yield: 0.018 g (30%). ^1H NMR (400 MHz, C_6D_6, 298 K): δ 7.33−7.27 (m, 6H, PC_6H_5), 6.98−6.88 (m, 9H, PC_6H_5), 6.79 (s, 2H, $C_6Me_3H_2$), 6.74 (s, 2H, $C_6Me_3H_2$), 6.18 (s, 2H, NC*H*), 2.18 (s, 6H, C−CH_3), 2.10 (s, 6H, C−CH_3), 1.96 (s, 6H, C−CH_3), −26.20 (ddd, $^2J_{HP}$ = 23.7 Hz, $^4J_{HF}$ = 6.0 Hz, $^4J_{HF}$ = 3.3 Hz, 1H, Ru-*H*). $^{13}C\{^1H\}$ NMR (101 MHz, C_6D_6, 298 K): δ 202.6 (br s, Ru-CO), 189.9 (d, $^2J_{CP}$ = 84 Hz, Ru-C_{NHC}), 138.8 (s, N-C_{ipso}), 136.9 (s, *p*-$C_6Me_3H_2$), 135.6 (s, *o*-$C_6Me_3H_2$), 135.5 (d, $^1J_{CP}$ = 39.5 Hz, P-C_{ipso}), 134.0 (d, J_{CP} = 11.8 Hz, PC_6H_5), 129.6 (d, J_{CP} = 1.6 Hz, PC_6H_5), 129.4 (d, J_{CP} = 3.1 Hz, PC_6H_5), 128.0 (s, *m*-$C_6Me_3H_2$), 127.9 (s, *m*-$C_6Me_3H_2$), 122.9 (s, NCH), 122.8 (s, NCH), 21.0 (s, CCH_3), 18.4 (s, CCH_3), 18.3 (s, CCH_3). $^{31}P\{^1H\}$ NMR (161 MHz, C_6D_6 298 K): δ 51.4 (d, $^2J_{PF}$ = 6 Hz). ^{19}F NMR (377 MHz, C_6D_6, 298 K): −102.9 (td, $^3J_{FF}$ = $^5J_{FF}$ = 30.1 Hz, $^4J_{FF}$ = 12.6 Hz, 1F), −104.8 (td, $^3J_{FF}$ = $^5J_{FF}$ = 31.9 Hz, $^4J_{FF}$ = 12.6 Hz, 1F), −116.0 (td, $^3J_{FF}$ = $^5J_{FF}$ = 30.1, $^4J_{FH}$ = 3.3 Hz, 1F), −123.7 (tt, $3J_{FF}$ = $^5J_{FF}$ = 31.9 Hz, $^4J_{FH}$ = $^4J_{FP}$ = 6.0 Hz, 1F). IR (KBr, cm^{-1}): 1932 (ν_{CO}). Anal. Calcd (%) for $C_{45}H_{40}N_3OF_4PRu$ (846.86): C, 63.82; H, 4.76; N, 4.96. Found: C, 63.63; H, 4.54; N, 5.04.

Procedure for Catalytic HDF Experiments. A J Young's resealable NMR tube was charged with **1** or **2** (0.01 M), fluoropyridine substrate (0.1 M) and Et_3SiH (0.2 M) in THF and a standardized capillary tube of a THF solution of α,α,α−trifluorotoluene inserted. An initial ^{19}F NMR spectrum was recorded and the tube heated to the required temperature in an oil bath. ^{19}F NMR spectra of the products were integrated relative to the internal standard and identified by comparison to authentic samples from commercial suppliers.

X-ray Crystallography. Single crystals of **3** were analyzed using a Nonius Kappa CCD diffractometer. Data were collected using Mo Kα radiation throughout. Details of the data collections, solutions, and refinements are given in the Supporting Information. The structure was solved using SHELXS-97[26] and refined using full-matrix least-squares in SHELXL-97.[26]

Crystallographic data for compound **3** has been deposited with the Cambridge Crystallographic Data Centre as supplementary publication CCDC 1021392. Copies of the data can be obtained free of charge on application to CCDC, 12 Union Road, Cambridge CB2 1EZ, U.K. [fax(+44) 1223 336033, e-mail: deposit@ccdc.cam.ac.uk].

Computational Details. DFT calculations were run with Gaussian 03 (Revision D.01)[27] and Gaussian 09 (Revision D.01).[28] Ru, P and Si centers were described with the Stuttgart RECPs and associated basis sets[29] with additional polarization on P (ζ = 0.387) and Si (ζ = 0.284)[30], and 6-31G** basis sets were used for all other atoms.[31] Initial BP86[32] optimizations were performed with Gaussian 03, with all stationary points being fully characterized via analytical frequency calculations as either minima (all positive eigenvalues) or transition states (one negative eigenvalue). IRC calculations and subsequent geometry optimizations were used to confirm the minima linked by each transition state. For each transition state, several possible orientations of the fluoropyridine moiety were tested and the most stable geometries/energies are reported in the main text. PCM corrections for the effects of THF solvent (ε = 7.43) were computed with Gaussian 09 and dispersion corrections applied using Grimme's D3 parameter set[33] using the BP86-optimized geometries. Functional dependency was assessed for a number of key stationary points via single point calculations with 15 different approaches (see Table S2, Supporting Information).

ASSOCIATED CONTENT

Supporting Information

The following files are available free of charge on the ACS Publications website at DOI: 10.1021/cs501644r.

DOI: 10.1021/cs501644r
ACS Catal. 2015, 5, 776−787

X-ray crystallographic data for **3** (CIF)
NMR spectra for **3**, phosphine exchange experiments for **1** and **2**, computed structures and energies for all computational results (PDF)

AUTHOR INFORMATION

Corresponding Authors

*Email: s.a.macgregor@hw.ac.uk.
*Email: m.k.whittlesey@bath.ac.uk.

Notes

The authors declare no competing financial interest.

ACKNOWLEDGMENTS

We acknowledge financial support from the EPSRC through grant numbers EP/J010677/1 (D.M.) and EP/J009962/1 (I.M.R.). We thank Dr Tim Woodman for help with NMR experiments and Johnson Matthey PLC for the loan of hydrated $RuCl_3$.

REFERENCES

(1) (a) Müller, K.; Faeh, C.; Diederich, F. *Science* **2007**, *317*, 1881−1886. (b) Hagmann, W. K. *J. Med. Chem.* **2008**, *51*, 4359−4369. (c) Kirk, K. L. *Org. Process Res. Dev.* **2008**, *12*, 305−321. (d) Purser, S.; Moore, P. R.; Swallow, S.; Gouverneur, V. *Chem. Soc. Rev.* **2008**, *37*, 320−330. (e) O'Hagan, D. *J. Fluor. Chem.* **2010**, *131*, 1071−1081. (f) Wang, J.; Sanchez-Rosello, M.; Luis Acena, J.; del Pozo, C.; Sorochinsky, A. E.; Fustero, S.; Soloshonok, V. A.; Liu, H. *Chem. Rev.* **2014**, *114*, 2432−2506.

(2) Kim, D.; Wang, L. P.; Beconi, M.; Eiermann, G. J.; Fisher, M. H.; He, H. B.; Hickey, G. J.; Kowalchick, J. E.; Leiting, B.; Lyons, K.; Marsilio, F.; McCann, M. E.; Patel, R. A.; Petrov, A.; Scapin, G.; Patel, S. B.; Roy, R. S.; Wu, J. K.; Wyvratt, M. J.; Zhang, B. B.; Zhu, L.; Thornberry, N. A.; Weber, A. E. *J. Med. Chem.* **2005**, *48*, 141−151.

(3) For recent reviews of metal-catalyzed HDF, see: (a) Kuehnel, M. F.; Lentz, D.; Braun, T. *Angew. Chem., Int. Ed.* **2013**, *52*, 3328−3348. (b) Whittlesey, M. K.; Peris, E. *ACS Catal.* **2014**, *4*, 3152−3159.

(4) (a) Kiplinger, J. L.; Richmond, T. G.; Osterberg, C. E. *Chem. Rev.* **1994**, *94*, 373−431. (b) Amii, H.; Uneyama, K. *Chem. Rev.* **2009**, *109*, 2119−2183. (c) Braun, T.; Wehmeier, F. *Eur. J. Inorg. Chem.* **2011**, 613−625. (d) Clot, E.; Eisenstein, O.; Jasim, N.; Macgregor, S. A.; McGrady, J. E.; Perutz, R. N. *Acc. Chem. Res.* **2011**, *44*, 333−348. (e) Johnson, S. A.; Hatnean, J. A.; Doster, M. E. *Prog. Inorg. Chem.* **2012**, *57*, 255−352. (f) Nova, A.; Mas-Ballesté, R.; Lledós, A. *Organometallics* **2012**, *31*, 1245−1256.

(5) Access to low F-containing products typically requires very forcing conditions and/or high catalyst loadings,[5a−d] although recent reports have employed alternative approaches using prior η^6-coordination of the arene[5e] or the synergistic action of two metal centers in a bimetallic complex:[5f] (a) Wu, J. J.; Cao, S. *ChemCatChem* **2011**, *3*, 1582−1586. (b) Fischer, P.; Götz, K.; Eichhorn, A.; Radius, U. *Organometallics* **2012**, *31*, 1374−1383. (c) Zhao, W. W.; Wu, J. J.; Cao, S. *Adv. Synth. Catal.* **2012**, *354*, 574−578. (d) Xiao, J.; Wu, J. J.; Zhao, W. W.; Cao, S. *J. Fluor. Chem.* **2013**, *146*, 76−79. (e) Gianetti, T. L.; Bergman, R. G.; Arnold, J. *Chem. Sci.* **2014**, *5*, 2517−2524. (f) Sabater, S.; Mata, J. A.; Peris, E. *Nat. Commun.* **2013**, *4*, 2553−2559.

(6) (a) Aizenberg, M.; Milstein, D. *Science* **1994**, *265*, 359−361. (b) Aizenberg, M.; Milstein, D. *J. Am. Chem. Soc.* **1995**, *117*, 8674−8675. (c) Vela, J.; Smith, J. M.; Yu, Y.; Ketterer, N. A.; Flaschenriem, C. J.; Lachicotte, R. J.; Holland, P. L. *J. Am. Chem. Soc.* **2005**, *127*, 7857−7870. (d) Yow, S.; Gates, S. J.; White, A. J. P.; Crimmin, M. R. *Angew. Chem., Int. Ed.* **2012**, *51*, 12559−12563. (e) Zhan, J.-H.; Lv, H.; Yu, Y.; Zhang, J.-L. *Adv. Synth. Catal.* **2012**, *354*, 1529−1541. (f) Li, J. Y.; Zheng, T. T.; Sun, H. J.; Li, X. Y. *Dalton Trans.* **2013**, *42*, 13048−13053. (g) Zámostná, L.; Ahrens, M.; Braun, T. *J. Fluor. Chem.* **2013**, *155*, 132−142.

(7) Johnson, S. A.; Huff, C. W.; Mustafa, F.; Saliba, M. *J. Am. Chem. Soc.* **2008**, *130*, 17278−17279.

(8) Reade, S. P.; Mahon, M. F.; Whittlesey, M. K. *J. Am. Chem. Soc.* **2009**, *131*, 1847−1861.

(9) For other ortho-selective systems of simple fluoroaromatics without directing groups, see: (a) Chen, Z.; He, C. Y.; Yin, Z. S.; Chen, L. Y.; He, Y.; Zhang, X. G. *Angew. Chem., Int. Ed.* **2013**, *52*, 5813−5817. (b) He, Y.; Chen, Z.; He, C. Y.; Zhang, X. G. *Chin. J. Chem.* **2013**, *31*, 873−877. (c) Podolan, G.; Lentz, D.; Reissig, H.-U. *Angew. Chem., Int. Ed.* **2013**, *52*, 9491−9494.

(10) Panetier, J. A.; Macgregor, S. A.; Whittlesey, M. K. *Angew. Chem., Int. Ed.* **2011**, *50*, 2783−2786.

(11) Macgregor, S. A.; McKay, D.; Panetier, J. A.; Whittlesey, M. K. *Dalton Trans.* **2013**, *42*, 7386−7395.

(12) NHC abbreviations: IPr = 1,3-bis-(2,6-diisopropylphenyl) imidazol-2-ylidene; IMes = 1,3-bis-(2,4,6-trimethylphenyl)imidazol-2-ylidene.

(13) For a review of computational work on C-F activation see : Algarra, A. G.; Macgregor, S. A.; Panetier, J. A. Mechanistic Studies of C-X Bond Activation at Transition-Metal Centers. In *Comprehensive Inorganic Chemistry II*, Reedijk, J., Poeppelmeier, E., Eds.; Elsevier: Oxford, 2013; Vol. *9*, pp 635−694.

(14) Reade, S. P.; Acton, A. L.; Mahon, M. F.; Martin, T. A.; Whittlesey, M. K. *Eur. J. Inorg. Chem.* **2009**, 1774−1785.

(15) Free energies for PPh_3/C_5F_5N exchange at 1 and 2 were computed to be +20.0 kcal/mol and +15.6 kcal/mol respectively at the BP86-D3(THF) level, but as reported by others,[15] these values show a significant functional dependence (see Table S2, Supporting Information). The precise free energy change for this pre-equilibrium will affect the overall barrier for HDF, although here we have focussed on the regioselectivity of the subsequent HDF process. (a) Minenkov, Y.; Occhipinti, G.; Jensen, V. R. *J. Phys. Chem. A* **2009**, *113*, 11833−11844.

(16) In comparison, the free energies for binding Et_3SiH or a THF solvent molecule at A are 8.0 and 0.3 kcal/mol, respectively.

(17) Hatnean, J. A.; Johnson, S. A. *Organometallics* **2012**, *31*, 1361−1373.

(18) (a) Nova, A.; Erhardt, S.; Jasim, N. A.; Perutz, R. N.; Macgregor, S. A.; McGrady, J. E.; Whitwood, A. C. *J. Am. Chem. Soc.* **2008**, *130*, 15499−15511. (b) Nova, A.; Reinhold, M.; Perutz, R. N.; Macgregor, S. A.; McGrady, J. E. *Organometallics* **2010**, *29*, 1824−1831.

(19) Huhmann-Vincent, J.; Scott, B. L.; Kubas, G. J. *Inorg. Chem.* **1998**, *38*, 115−124.

(20) (a) Holtcamp, M. W.; Henling, L. M.; Day, M. W.; Labinger, J. A.; Bercaw, J. E. *Inorg. Chim. Acta* **1998**, *270*, 467−478. (b) Basu, S.; Arulsamy, N.; Roddick, D. M. *Organometallics* **2008**, *27*, 3659−3665. (c) Adams, J. J.; Arulsamy, N.; Roddick, D. M. *Organometallics* **2009**, *28*, 1148−1157. (d) Bowring, M. A.; Bergman, R. G.; Tilley, T. D. *Organometallics* **2013**, *32*, 5266−5268.

(21) A higher energy transition state (G = +20.7 kcal/mol) was also located in which the C^2−F^2 lies perpendicular to the Ru-NHC bond.

(22) Other examples of this type of hydride attack mechanism proceding with *para*-selectivity at C_5F_5N have been reported, see: (a) Beltrán, T. F.; Feliz, M.; Llusar, R.; Mata, J. A.; Safont, V. S. *Organometallics* **2011**, *30*, 290−297. (b) Lv, H.; Cai, Y.-B.; Zhang, J.-L. *Angew. Chem., Int. Ed.* **2013**, *52*, 3203−3207.

(23) Ojima, I. *Fluorine in Medicinal Chemistry and Chemical Biology*; Wiley-Blackwell: Chichester, U.K., 2009.

(24) In our previous C_6F_5H studies[10,11] a Ru-C_6F_4H fluoroaryl intermediate was located which underwent facile protonolysis by HF released in the C−F bond cleavage step. For *meta*- and *para*-HDF with C_5F_5N, no equivalent Ru-C_5F_4HN intermediate was located and IRCs showed **TS(B-C)3** led directly to **D** + the free C_5F_4HN product.

(25) Analogous structures to **Int(B-C)2′** can be located for the IPr system with G = +3.0 kcal/mol and +11.2 kcal/mol for *para*- and *meta*-HDF respectively. However, in these cases, they do not link to **TS(B-C)3** and so do not lie directly on the HDF reaction profile.

(26) (a) Sheldrick, G. M. *Acta Crystallogr., Sect. A* **1990**, *46*, 467−473. (b) Sheldrick, G. M. *SHELXL-97, a computer program for crystal*

DOI: 10.1021/cs501644r
ACS Catal. 2015, 5, 776−787

structure refinement; University of Gottingen: Gottingen, Germany, 1997.

(27) Frisch, M. J.; Trucks, G. W.; Schlegel, H. B.; Scuseria, G. E.; Robb, M. A.; Cheeseman, J. R.; Montgomery, J. A., Jr.; Vreven, T.; Kudin, K. N.; Burant, J. C.; Millam, J. M.; Iyengar, S. S.; Tomasi, J.; Barone, V.; Mennucci, B.; Cossi, M.; Scalmani, G.; Rega, N.; Petersson, G. A.; Nakatsuji, H.; Hada, M.; Ehara, M.; Toyota, K.; Fukuda, R.; Hasegawa, J.; Ishida, M.; Nakajima, T.; Honda, Y.; Kitao, O.; Nakai, H.; Klene, M.; Li, X.; Knox, J. E.; Hratchian, H. P.; Cross, J. B.; Bakken, V.; Adamo, C.; Jaramillo, J.; Gomperts, R.; Stratmann, R. E.; Yazyev, O.; Austin, A. J.; Cammi, R.; Pomelli, C.; Ochterski, J. W.; Ayala, P. Y.; Morokuma, K.; Voth, G. A.; Salvador, P.; Dannenberg, J. J.; Zakrzewski, V. G.; Dapprich, S.; Daniels, A. D.; Strain, M. C.; Farkas, O.; Malick, D. K.; Rabuck, A. D.; Raghavachari, K.; Foresman, J. B.; Ortiz, J. V.; Cui, Q.; Baboul, A. G.; Clifford, S.; Cioslowski, J.; Stefanov, B. B.; Liu, G.; Liashenko, A.; Piskorz, P.; Komaromi, I.; Martin, R. L.; Fox, D. J.; Keith, T.; Al-Laham, M. A.; Peng, C. Y.; Nanayakkara, A.; Challacombe, M.; Gill, P. M. W.; Johnson, B.; Chen, W.; Wong, M. W.; Gonzalez, C.; Pople, J. A. *Gaussian 03*, revision D.01; Gaussian, Inc.: Wallingford CT, 2004.

(28) Frisch, M. J.; Trucks, G. W.; Schlegel, H. B.; Scuseria, G. E.; Robb, M. A.; Cheeseman, J. R.; Scalmani, G.; Barone, V.; Mennucci, B.; Petersson, G. A.; Nakatsuji, H.; Caricato, M.; Li, X.; Hratchian, H. P.; Izmaylov, A. F.; Bloino, J.; Zheng, G.; Sonnenberg, J. L.; Hada, M.; Ehara, M.; Toyota, K.; Fukuda, R.; Hasegawa, J.; Ishida, M.; Nakajima, T.; Honda, Y.; Kitao, O.; Nakai, H.; Vreven, T.; Montgomery, J. A., Jr.; Peralta, J. E.; Ogliaro, F.; Bearpark, M.; Heyd, J. J.; Brothers, E.; Kudin, K. N.; Staroverov, V. N.; Kobayashi, R.; Normand, J.; Raghavachari, K.; Rendell, A.; Burant, J. C.; Iyengar, S. S.; Tomasi, J.; Cossi, M.; Rega, N.; Millam, J. M.; Klene, M.; Knox, J. E.; Cross, J. B.; Bakken, V.; Adamo, C.; Jaramillo, J.; Gomperts, R.; Stratmann, R. E.; Yazyev, O.; Austin, A. J.; Cammi, R.; Pomelli, C.; Ochterski, J. W.; Martin, R. L.; Morokuma, K.; Zakrzewski, V. G.; Voth, G. A.; Salvador, P.; Dannenberg, J. J.; Dapprich, S.; Daniels, A. D.; Farkas, O.; Foresman, J. B.; Ortiz, J. V.; Cioslowski, J.; Fox, D. J. *Gaussian 09*, revision D.01; Gaussian, Inc.: Wallingford CT, 2013.

(29) Andrae, D.; Häußermann, U.; Dolg, M.; Stoll, H.; Preuß, H. *Theor. Chim. Acta* **1990**, *77*, 123−141.

(30) Höllwarth, A.; Böhme, M.; Dapprich, S.; Ehlers, A. W.; Gobbi, A.; Jonas, V.; Köhler, K. F.; Stegmann, R.; Veldkamp, A.; Frenking, G. *Chem. Phys. Lett.* **1993**, *208*, 237−240.

(31) (a) Hehre, W. J.; Ditchfield, R.; Pople, J. A. *J. Chem. Phys.* **1972**, *56*, 2257−2261. (b) Hariharan, P. C.; Pople, J. A. *Theor. Chim. Acta* **1973**, *28*, 213−222.

(32) (a) Perdew, J. P. *Phys. Rev. B* **1986**, *33*, 8822−8824. (b) Becke, A. D. *Phys. Rev. A* **1988**, *38*, 3098−3100.

(33) Grimme, S.; Antony, J.; Ehrlich, S.; Krieg, H. *J. Chem. Phys.* **2010**, *132*, 154104−1−154104−19.

DOI: 10.1021/cs501644r
ACS Catal. 2015, 5, 776−787